Additive Manufacturing xxx (xxxx) 102320

Contents lists available at ScienceDirect

Additive Manufacturing

journal homepage: www.elsevier.com/locate/addma

Research paper

Predicting interfacial layer adhesion strength in 3D printable silicone

Stephanie Walker [a,*], Emma Lingle [a], Natasha Troxler [a], Thomas Wallin [b], Katherine Healy [b], Yiğit Mengüç [b], Joseph Davidson [a]

[a] CoRIS Institute, Oregon State University, 204 Rogers Hall, Corvallis, OR 97331, USA
[b] Facebook Reality Labs, Redmond, WA, USA

ARTICLE INFO

Keywords:
Adhesion
Peel testing
Silicone
Direct ink writing
3D printing
Additive manufacturing

ABSTRACT

Direct ink writing is an excellent method for depositing soft elastomeric silicones into a 3D shape, as shown by several examples in the current literature. However, further investigation into the quality of these 3D printed parts is required to ensure this process can be reliable. Especially for fields like soft robotics, where these printed silicone parts are inflated and the bulk material is in tension, interfacial layer adhesion is integral to the ultimate tensile robustness of a part and preventing premature failure. Interfacial layer adhesion changes based on the cure state of the previously deposited silicone layer, which can change based on amount of cure retarding additives, when the material was last mixed, and the temperature of the printing chamber. Yet, interfacial layer adhesion between printable silicone has not yet been characterized in the literature. This work seeks to rectify that by quantifying the relationship between curing kinetics, tested using differential scanning calorimetry, and peel testing of a printable Ecoflex 00-30 based silicone formulation. These data show a negative correlation between cure percent and interfacial adhesion force with values usable for prediction of printed part tensile strength. These data are then implemented into a G-code visualization tool to display the interfacial adhesion quality based on CAD model geometry and print speed. This work shows that cure percent has to be incorporated into direct ink write path planning to ensure control of the part's final tensile behavior.

1. Introduction

Direct ink writing is one method of 3D printing soft liquid polymers and other fluids. Liquid precursors are extruded into 3D shapes that then undergo subsequent chemical crosslinking reactions, or other post-processing, to produce a finished three-dimensional part. Use of thermosetting elastomers for direct ink writing is an active field of research in several applications, including the creation of multi-material voxelated (made into 3D equivalents of pixels) parts [1], control of printed resolution using fluid deformation/instability/fracture [2], exploration of mixing techniques [3], printing of soft materials into a supportive bath [4–6], extrusion of multi-layered concentric sensors [7], silicone extruded fluid patterning [8], printing with silicone microbeads [9], printing silicone onto a 3D surface [10,11], tuning 3D printable silicone material properties [12], multi-material printing with silicone and wax [13], and developing zero-support 3D printing methods for soft silicone [14].

Generally, direct ink writing materials are difficult to 3D print without some rheological modification(s) or support bath structures due to their inherent softness and low viscosity. Material design must ensure uninterrupted flow through the printing nozzle and substantive strength after extrusion for 3D layering and overhanging geometries. Rheological modifications generally increase the yield stress, control the viscoelastic parameters like elastic modulus (G´), control viscosity, and promote shear thinning [15] in the inks. A high yield stress prevents slumping and collapse of the extruded material during printing. The material is ideally G´ dominated for solid-like (versus liquid-like) behavior in the fluid, but G´ should not be so high as to prevent extrusion entirely. Shear thinning properties in the fluid align the polymer chains in high shear regions like the nozzle to lower the viscosity for lower pressure extrusion.

Direct ink writing of thermosetting elastomers requires another important modification to either the printed fluid or the printing process – control of the curing kinetics. Polymers are either slow-curing or premixed with a cure retarder (such as an organic or organosiloxane additive) [16] to prevent material clogging the nozzle, or, mixed just before extrusion to quickly push the curing material out of the nozzle before it begins to solidify. Direct ink writing of curing thermoset elastomers is a

Abbreviations: DIW, (direct ink writing); DSC, (differential scanning calorimetry); LSR, (liquid silicone rubber); RTV-2 (, room temperature vulcanizing, 2-part)

* Corresponding author.
E-mail addresses: walkers@oregonstate.edu (S. Walker), joseph.davidson@oregonstate.edu (J. Davidson).

https://doi.org/10.1016/j.addma.2021.102320
Received 26 May 2021; Received in revised form 31 August 2021; Accepted 10 September 2021

non-trivial process if curing speed is not slowed down. A changing cure rate during printing correlates with changing rheological properties, such as growth of G´ [14] and increase in viscosity, which can clog the nozzle. Increasing the temperature of the curing thermoset will also increase the cure rate, so the temperature environment should be strictly controlled to reduce variability in the rheological and curing behavior.

Managing curing kinetics, rheology, and temperature are necessary for a dependable thermoset direct ink writing process. Previous work [14] developed a framework for characterizing these parameters for arbitrary thermoset materials, developed formulation strategies, rheological control, curing kinetics characterization, and geometrical design rules for implementation in a custom-built active mixing 3D printer. The printer incorporated an in-line mixer to actively mix two parts of a custom RTV-2 (room temperature vulcanizing, 2-part) silicone just before extrusion in a heated chamber, and therefore maintained strength as the subsequent layers were deposited. This printing process also permitted a greater degree of control over the silicone's curing process without the need to chemically alter the cure speed of the silicone. The elevated temperatures ensured that previously printed layers rapidly cured and therefore developed more strength as the print progressed until they reached a solid state. This structure development allowed overhanging features (up to 45 degrees), inaccessible in conventional systems, to hold their shape during printing. To prevent curing in the mixer and nozzle while also increasing the cure speed of layers as much as possible, the system was characterized for curing kinetics and rheology to define an optimal printing time window and maximum operating temperature. But, while zero-support overhanging structures could be made with liquid silicone rubber (LSR), this investigation did not assess the effects of layer curing on final device performance.

We have created a new silicone formulation based on Ecoflex 00-30 using the techniques developed in [14]. This silicone has been used to 3D print several examples including single-wall cylinders, overhang wedges, and spanning filaments. This formulation has shown its ability to hold structure right out of the mixer by spanning several millimeters without breakage (with an approximately 0.5 mm diameter filament) and by stacking right after deposition in a single-layer thickness (approximately 1 mm filament) wall (see Video A1). Fig. 1 shows a close-up of the in-line mixer and three printed examples using this formulation.

Supplementary material related to this article can be found online at doi:10.1016/j.addma.2021.102320.

Theoretically, as each printed layer cures over time, there are fewer crosslinkable groups available for bonding to the subsequent layer. The build time for each layer is dependent on its cross-sectional area, so individual layers may experience drastically different layer deposition times, and therefore, extent of curing reaction, before the deposition of the next silicone layer. Inadequate crosslinking between layers can lead to anisotropy and premature failure, i.e., delamination at stresses below the ultimate strength of the base material. The interfacial force is integral to predictable mechanical performance and therefore predictability of the direct ink writing process.

Maximizing interfacial adhesion between two printed layers is integral to achieving maximum part tensile strength. However, when 3D printing curing silicones, the adhesion between printed lines composing an object becomes more complex. Silicone printing cannot necessarily use the same flow math as seen in Slic3r (one G-code generator software), [17] which uses the cross-sectional line shape of a rectangle sided by two hemispheres (Fig. 2a). The basic shapes seen in preliminary EF profilometry characterization are shown in Figs. 2b–d. A single-line printed on glass has a hemispherical cross-section (Fig. 2b). The quality of 3D printed silicone is highly situational based on geometry of the model, G-code settings, temperature, and pump flow rate. For example, in an unoptimized system with a single wall thickness printed right out of the mixer (Fig. 2c), uncured lower layers can deform under the weight of the deposited layers above, and those deposited layers form a hemispherical stack lower than the height of the CAD model. However, in an system optimized for layer height printed right out of the mixer with layer height, width, and print speed properly chosen (Fig. 2d) an acceptable height can be achieved, though some edge distortions occur due to silicone flow. Fig. 2d the ideal height is 1.5 mm and the actual height (averaged across three areas of the cross-section × 5 sample cross sections) is 1.54 +/- 0.060 mm (Appendix). Printed EF also benefits from slightly more material being printed than needed so it can fill the shape properly, similar to traditional thermoplastic materials printed with Slic3r [17]. Each printed line has six potential idealized surfaces available for adhesion (top, bottom, left, right, start, end) (example in Fig. 2e) that should be considered during path planning development.

Other considerations for silicone 3D printing include line horizontal overlap that makes determining interfacial horizontal surface area difficult (Fig. 2f). Peel testing samples as-printed is difficult in a system still being developed for optimal fidelity. Testing the material directly, outside of the printing procedure, gives an ideal peel behavior based on a well-known testing method, without needing to adjust for unusually shaped surface areas. This also allows for larger samples to be tested, instead of peeling thin lines which would require more sensitive force gauges. Peel testing outside of the printing system first is a better predictor of performance than a printing procedure highly dependent on mixing quality, flow quality, nozzle acceleration, and single- and multiple-line geometry.

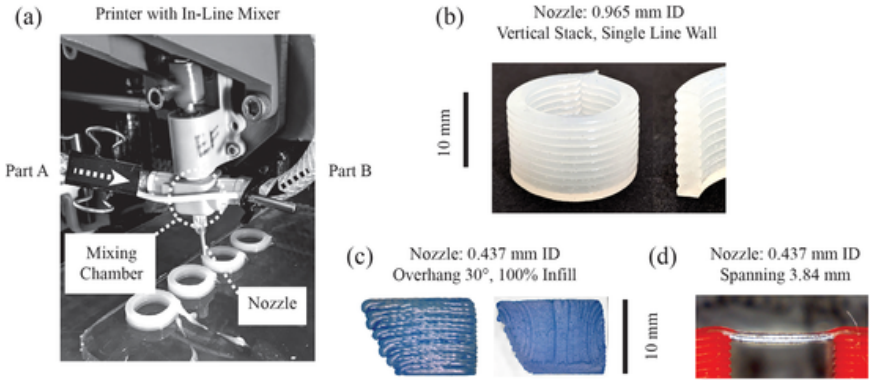

Fig. 1. Printed models using the new Ecoflex (EF) based formulation. (a) Close-up of the in-line mixer. (b) A 10 mm high single-walled cylinder printed with a 0.965 inner diameter nozzle. (c) A 10 mm high 30° overhang (from the vertical) wedge from the exterior side view (left) and the filled interior cut cross-sectional view (right), printed using a 0.437 mm inner diameter nozzle. (d) A cured spanning sample printed using a 0.437 mm nozzle showing the EF filament crossing a 3.84 mm gap without support. Spanning filaments were deposited right after exiting the mixer.

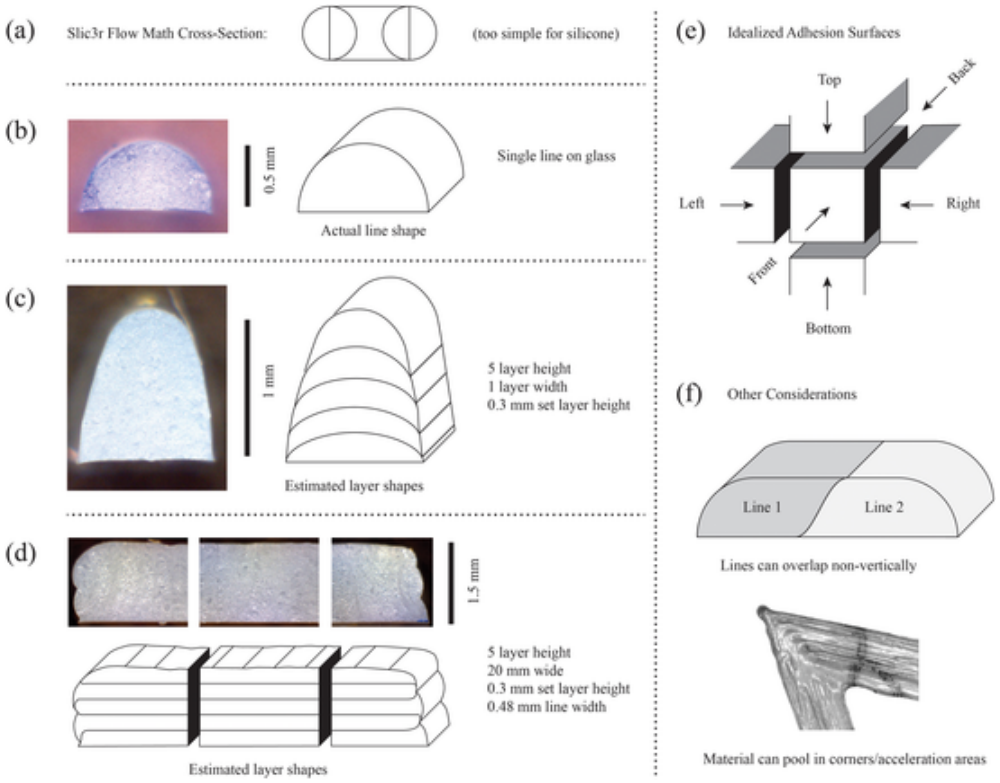

Fig. 2. Adhesion considerations for the current EF printing system. (a) Traditional Slic3r flow math used for thermoplastic filaments like PLA, which are not necessarily applicable to EF. (b) Actual cross-sectional profile of single EF line extruded onto glass build plate from a 0.437 mm inner diameter nozzle. (c) Actual cross-sectional profile of an unoptimized five layer single-line EF stack extruded from the same nozzle. (d) Three actual cross-sectional profiles of an optimized multiple-line sample. (e) Idealized adhesion surfaces to consider when designing path-planning algorithms for G-code generation. (f) Other considerations when printing include non-vertical overlap in adjacent lines and overfill during acceleration.

3D parts with complex geometry will require custom path planning strategies to include the cure percent and expected interfacial adhesion force in the polymer deposition pattern. Path planning is straightforward for single-wall prints comprised of a single stack of lines. However, in most cases, each printed layer will contain a complex mixture of wall thicknesses and number of lines in the cross-section, making path planning complex when accounting for all contact surfaces in the print. This printing system requires many types of characterization to ensure a quality print, including geometrical fidelity under a range of printing conditions. But, during this developmental phase, adhesion is one important parameter worth investigating for the overall printer development.

This work expands upon the existing framework [14] for direct ink writing of a thermoset silicone by correlating the peel strength of silicone with its cure percent. We developed a new silicone formulation for printing with Ecoflex 00-30 (EF) and additives, characterized the formulation's rheology, and determined its suitability for printing (characterization included in the Appendix). This thermoset silicone is used to explore how curing kinetics affect adhesion strength in a direct ink writing material. Isothermal differential scanning calorimetry (DSC) was performed for three possible printing temperatures to determine a range of timings for the silicone curing kinetics. The printing temperature (60 °C) in this system was determined within these ranges by running multiple prints in the printer system at temperature without clogging. Because the printer technology is still in development, adhesion samples were mixed outside of the printing system in a planetary centrifugal mixer to ensure "perfect" mixing for characterization. Samples were created using timed film spreading of two layers inside the printer chamber to control the cure percent of the bottom layer before the addition of the top layer. Interfacial adhesion forces were determined using a modified T-Peel test method. The data show that a low cure percent before new layer deposition leads to higher strength parts, and higher cure percent before new layer deposition leads to lower strength parts. While these results may seem straightforward to those familiar with polymer curing processes, adhesion data for layered silicone in DIW is missing in the current literature. These peel force data are incorporated into a predictive G-code visualizer to display the adhesion quality of an example printed model based on print speed and dimensions. This process can be further iterated upon in DIW to improve part predictability, especially with regards to peel or tensile failure.

1.1. Background

Platinum cure silicone chemistry is typically an addition reaction (hydrosilylation) between two prepared and mixed parts with no byproducts [18]. This type of reaction produces a crosslinked thermoset silicone connected via covalent bonds. In silicones like the RTV-2 Ecoflex 00-30, as temperature increases, the rate of crosslinking also increases, enabling thermal control of the curing kinetics. Before the silicone is fully cured and (theoretically) all precursors have been crosslinked into a polymer structure, there are unreacted precursors still in the mixture, which diffuse through the network to react with one another [19]. If the silicone is isothermal and above a few microns in thickness [20], all of the material should have the same curing kinetics. Differential scanning calorimetry is a common method of determining cure percent (α) [21–23]. Isothermal DSC data (Watts/gram of sample

versus time) is used to calculate the rate of cure using the instantaneous heat flow divided by the total heat integral under the heat flow curve. A running integral of the heat flow data divided by the total heat integral gives the cure percent [24]. Because each bonding process releases a specific amount of energy, it is assumed that heat flow is directly proportional to cure percent [25].

The types of adhesion possible between layers during the curing phase of an addition cure silicone depend on the specific chemistry, but generally include covalent bonding between the reactive sites (in this case, even though the Ecoflex formulation is proprietary, vinyl ($-CH=CH_2$) and silicon hydride (Si-H) groups are expected) based on platinum-curing silicone chemistry, and intermolecular (Van der Waals) bonds between all parts of the mixture (dipole-dipole, London dispersion, induced dipole, and hydrogen bonds). Additives included in the formulation (ex: silica) also can affect adhesive material properties based on their aggregation, pore volume, and polymer-filler attachments [26,27]. Polymer chain entanglements also can serve as effective crosslinks, adding to overall adhesion [28]. Adhesion is also dependent on processing conditions such as the interfacial surface area available for contact, which changes in the presence of imperfect deposition such as air pockets or irregular surfaces.

Quantifying the exact types of adhesive forces in the curing layers is beyond the scope of this work, but it is assumed that the more crosslinking that occurs at an interface, the more that the interface will resist peeling apart due to the formation of more covalent bonds. Cure percent can be correlated to adhesive peel strength in the silicone layers (Fig. 3). A T-Peel test characterizes this correlation by quantifying the peel resistance via adhesion forces (force/width of sample) between the two layers [29]. The data from the T-Peel test generally show a peak of initiation force followed by a range of crack propagation forces that peel the sample until break. Peel sample geometry, plastic or elastic deformation in the peel arms/tabs, energy dissipation effects, material composition, temperature, separation rate, interface effects, test angle, and equipment can affect peel test results [30–33]. The initiation of the peel also has its own complexities depending on the sharpness of the crack and the types of stress distributions at the crack front [31]. The ideal failure mode in a printed or layered part is 100% cohesive failure, in which the adhesive bond is strong enough to cause the bulk material to break before peeling at the interface, ideally using the maximum strength of the material. Adhesive failure (occurring only at the interface) means that the weakest area of the printed part is between printed layers. A mixture of cohesive and adhesive failure can also occur [34].

While previous work in direct ink writing of thermosets focused on rheological modifiers and altering reaction rates for rapid shape fixity, the impact on interlayer adhesion remains unclear. Past work has assumed proper layer adhesion as long as the layers were deposited before the silicone fully cured [35], relied on full curing of the previous layer before a new layer was deposited to ensure adequate structural integrity [36], or did not focus on layer adhesion in the work [14]. Layer-to-layer adhesion research is more common in stereolithography printing, where ultraviolet (UV) or infrared (IR) light is passed through a layer of uncured resin or a focused voxel within a bath to build 3D structures [37]. Silicone has been 3D printed with these methods [38,39]. The bonding between layers is permanent, and light bleed-through from the curing layer to the previously irradiated layer creates a layer-to-layer bond [40,41]. The amount of cure depends on the light intensity, exposure time, as well as the specific polymer chemistry [42]. In UV-cured chemistry as well as the thermoset chemistry presented here, control of the curing kinetics is integral to proper printed part strength and dimensional accuracy.

Silicone adhesion between layers also has implications for soft device fabrication outside of 3D printing. Soft lithography is a common method to adhere two silicone parts together. Often, a newly-mixed and uncured silicone is used as an adhesive for two or more silicone parts [43–45]. While the maximum strength of adhesion is not usually tested, it is assumed that the adhesion between the cured and uncured silicone is sufficient for the intended task. This type of adhesion is especially important to quantify in inflatable structures which often fail at these glued seams. Knowing the point of failure before building a soft device is an important step to improving its manufacturing process.

2. Material and methods

2.1. Silicone preparation

Ecoflex 00-30 (EF) (Smooth-On, USA) was used as the base polymer. Thi-Vex and Urefil-9 (both from Smooth-On, USA) were added, resulting in the following mixtures: (Part A) 44.5 g EF Part A, 0.5 g TV, 1.0 g Urefil-9 and (Part B) 44.5 g EF Part B 0.5 g TV, 1.0 g Urefil-9. Thi-Vex is a thixotropic additive and thickener which increases viscosity, and Urefil-9 is a fumed silica-based thickening agent. These additives ensure the EF mixture has a high enough viscosity and yield stress to hold its shape during printing. Each component (Part A Mixture and B Mixture) was mixed in a Thinky ARE-310 planetary mixer for 30 s at 2000 rpm and 30 s at 2200 rpm. The mixed parts were then loaded into their separate syringes using a spatula. Part A and Part B were used for DSC tests as-is. To remove bubbles from this highly viscous yield stress fluid for film spreading, a few additional steps were taken. First, each full syringe was divided into two syringes by extruding half the volume of one syringe into a new syringe. Second, the syringe plungers were com-

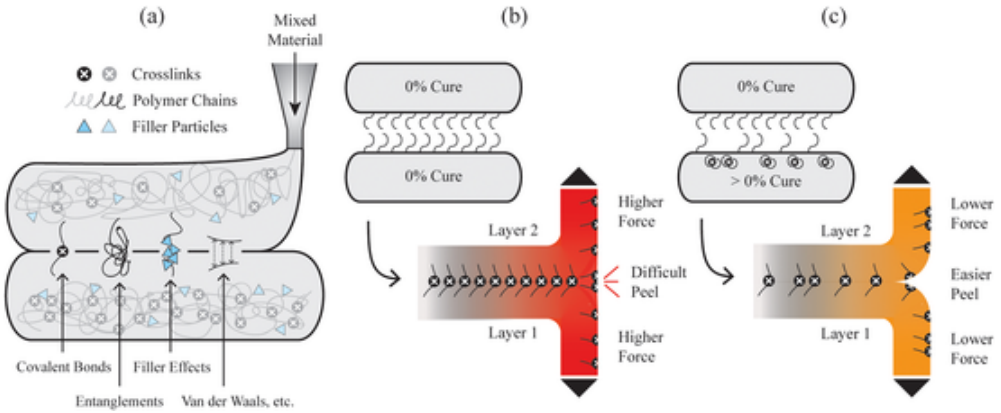

Fig. 3. Adhesion between printed layers. (a) Conceptual drawing of some adhesion contributors between curing layers during 3D extrusion and layering. (b) General crosslinking and peeling behavior between two uncured layers. (c) Expected general crosslinking and peeling behavior of two layers, with one layer being partially cured.

pressed to push all the material towards the syringe tip, and then quickly removed to spread the material over the inner walls of the syringe. Vacuuming out the bubbles from the thin layer of material on the walls of the syringe was easier than in a large volume in a cup. The syringes were vacuumed without plungers for 30 min, and then the plungers were replaced and two syringes (of the same Part A or B) were recombined into one syringe for experiments. Experiments to ensure initial printability of the formulation are detailed in Fig. A1–A5 in the Appendix.

2.2. Curing kinetics testing

Curing kinetics of the thermoset silicones were determined on a DSC Q2000 (TA instruments) using isothermal temperature scans. Approximately 2 g Part A and 2 g Part B were mixed in a Thinky ARE-310 Planetary mixer for 2000 rpm for 15 s and then 2200 rpm for 15 s at room temperature. The sample was then quickly loaded into a new 1 mL syringe with an attached nozzle and extruded into the hermetic pan, noting the mass of the sample. Sample masses ranged from 13.8 mg to 18.7 mg. The lid was then quickly crimped onto the pan and the sample was loaded into the pre-heated DSC, approximately 2 min from mixing. The sample (silicone + aluminum hermetic pan and lid) and reference (aluminum hermetic pan and lid only) were placed in the isothermal furnace for approximately 30 min and heat flow coming from the sample pan was recorded over time. Testing temperatures in the furnace (50 °C, 60 °C and 70 °C) were chosen based on previous experience printing these types of silicones and knowledge of the printer system's print speed capabilities. Five samples were run per temperature and averaged. The heat flow curves represent the heat given off by the sample during curing, with exothermic data in the positive direction. It was assumed that every bond made in the curing silicone released the same amount of exothermic heat, and so the heat flow of the sample was proportional to the cure rate. The isothermal silicone samples generally had a heat flow curve that grew into a peak and then decreased until reaching a region of no heat flow change. The beginning of the region with no heat flow change at the end of the run was the cure point (with the assumption of no additional reactions). Because of the assumption of proportionality described earlier, the maximum of the heat flow peak was also the maximum cure rate. The data for EF at a variety of estimated printing temperatures was presented, with one print temperature chosen for peel sample preparation based on operator safety when using higher temperatures in the chamber as well as speed of printing possible in the printing system without clogging.

2.3. Peel testing

2.3.1. Peel sample preparation

The heated chamber of the printer was used to spread the silicone films within an isothermal environment. The system consists of three PID controlled space heaters with fans to circulate the air, all within an insulated box. The printing chamber and printer bed (Luzbot Taz 6) were heated to 60 °C. Two thermocouples were placed in the center of the chamber, one near the extrusion nozzle and one slightly above it on the camera boom, and their temperature results were averaged. For all sample runs the air temperature was 60.2 ± 0.45 ºC. A thick glass plate was set on top of the bed to provide a more homogeneous temperature surface because the build plate alone tended to unevenly distribute heat.

For clarity, the following procedure for preparing peel test samples is illustrated in Fig. A6 in the Appendix. To prepare the peel test samples, approximately 6.5 g of Part A Mixture and 6.5 g of Part B Mixture were extruded from their respective syringes at room temperature into separate sides of one mixing cup so that the two parts did not touch. Two of those cups were pre-heated inside the printing chamber for at least 20 min. The first pre-heated cup was then placed into the Thinky ARE-310 Mixer and a timer was started. After mixing for 15 s at 2000 rpm and 15 s at 2200 rpm, the mixed silicone was quickly scooped onto the bed in front of a razor blade lifted 2 mm from the bed. The first layer of the sample was spread across approximately 100 mm of length and 30 mm width, and a pre-cut acetate layer was placed down near the end of the spread film to prevent that region's adhesion to the next layer. Each cup mixing process took about 85 s, so the second pre-heated cup was placed in the mixer 85 s before the desired time elapsed (2.75, 4, 6, 8, 12 or 16 min). After mixing, the second sample was then scooped onto the same region as before but on top of the previous layer, and spread across the existing bottom layer using a razor blade lifted 4 mm from the bed. The 2-layer sample sheet was then left to cure for 12 min at 60 °C, and then removed from the glass plate. All samples were post-cured in an 80 °C oven for one hour. The next day, the sample sheets were cut by hand with a steel ruler and razor blade into approximately 6.5 mm wide strips with 75 mm of adhered region past the acetate tab boundary. Sil-Poxy was then spread on both sides of the outer tab areas to help improve clamp grip during testing. The acetate masks were gently removed from each sample before loading into the tensile tester. Images of the printer chamber and heated plate are shown in Fig. A7 in the Appendix.

2.3.2. Peel sample testing

Sample test methods were based on ASTM D1876-08: Standard Test Method for Peel Resistance of Adhesives (T-Peel Test). Two strips of material were pulled apart from an initially T-shaped sample using a custom-built tensile testing machine (Fig. A8, Appendix). Samples were loaded into the testing machine connected to a 10 kg (~98 N) load cell. The sample tabs were placed into the upper and lower grips and tightly secured. The tester then pulled the layers apart at 100 mm/min until complete separation. At least seven samples were tested per cure time. The data recorded were force, time, and extension. Force data was normalized to the average width of each sample interface. Average width was determined by taking three measurements of the interface using a microscope with a micrometer and then averaging the results (Fig. A9, Appendix). Force per width versus extension data were plotted for each sample (Fig. A10, Appendix) and an average adhesion force across the entire extension region was calculated after the initiation peak and before the break. Average adhesion force was then plotted versus time difference between printed layer deposition.

2.4. G-code peel strength visualizer design

A G-code Peel Strength Visualizer (GPSV) was developed in MATLAB to assign and visualize peel force values to points in the G-code of a sample single layer walled CAD model. This code does not address horizontal adhesion between filaments or the adhesion path planning required to fill in a solid model, but is a start for increasing understanding of the importance of peel force data in this type of 3D printing. Peel force values were separated into three regions: "safe", "transitional", and "unsafe" based on the peel force data range. The safe range was from 0 to 4 min (just before the force noticeably dropped), the transitional range was from 4 to 5.71 min, and the unsafe range was from 5.71 min. The time boundary between the transitional and unsafe region was the first time along the interpolated curve from 4 to 5.71 min associated with the maximum force value for all peel tests from 6 to 16 min. G-code was created for a single-walled CAD model using Simplify3D. All G-code x, y, and z values were brought into MATLAB and run through the algorithm that first separated the G-code points into layers. Interpolated points were added between each G-code point to increase the number of searchable points from layer-to layer. An iterative process was used to determine the time from a point on a chosen start layer to the nearest point on the layer above. Each layer was designated as "Layer A" if the chosen layer and "Layer B" if the layer just above Layer A. The algorithm finds one nearest point on Layer B for each point

on Layer A and then calculates the distance from point to point along the G-code path. This value divided by the desired print speed gives the point-to-point time which is compared to the peel force data. The point-to-point peel force is designated on Layer B using a color representing one of the three peel force quality regions. This color indicates the peel force that the Layer B point would show in relationship to the point on Layer A. This process is iterated across all points on Layer A to B, and then the next Layer A (previously Layer B) is run through the algorithm with a new Layer B. All code for the GPSV is available in the Appendix. This visualization is useful for understanding the role of exterior CAD model geometry in final peel strength. More complex visualizations of fully filled and multiple perimeter CAD models are left to future work.

3. Results

3.1. Curing kinetics

Isothermal DSC testing at 50, 60, and 70 °C gave cure rate ($d\alpha/dt$) curves with average peak cure rates occurring at 16.4, 6.6, and 3.0 min, respectively. Total cure times for those same temperatures were 21.5, 10.3, and 5.8 min (Fig. 4 left). Running integrals of the cure rate curves gave cure percent curves (Fig. 4 right). These curves are later used to compare cure percent with adhesive force between layers.

3.2. Peel testing

Peel testing of all samples revealed a region of higher peel forces occurring at 2.75 and 4 min, (0% and 0.4% cure, respectively) and a region of lower peel forces at 6, 8, 12, and 16 min (24%, 90%, 100%, and 100% cure, respectively). Fig. 5 (left) shows the force/width data for all samples. Lighter lines in Fig. 5 (left) show the initiation peak and the end data; darker lines show the data after the initial peak (the initiation of the peel) and before break. The data are separated by cure time on the plot for clarity. A boxplot analysis of the data is shown in Fig. 5 (right). All peel test data is shown in the Appendix. Clear groupings occur in the data means at $<=4$ min and $>=6$ min. Table 1 shows the average maximum and average mean peel force values of each cure time data set. The maximum value for each sample time in the table is the mean maximum force/mm of all data in the respective set including the initiation peak. The average mean value for each sample time in Table 1 is the mean value of all means in the respective set. Average maxima for the high force region range from 0.382 N/mm to 0.392 N/mm. Average maxima for the low force region range from 0.270 N/mm to 0.358 N/mm. Average means from the high force region range from 0.307 N/mm to 0.310 N/mm. Average means from the low force region range from 0.235 N/mm to 0.253 N/mm.

Failure modes of the peel test samples depend on the cure time between the two peeled layers. Fig. 6 (left) shows the overall percentages of cohesive failure (failure in the bulk material) of each sample type. In Fig. 6 (right) two images show the difference between a sample that experienced cohesive failure and a sample that experienced adhesive failure. All samples with interfacial time differences of 8, 12, and 16 min underwent adhesive failure only.

3.3. G-code peel strength visualizer results

The GPSV was implemented using a single layer wide G-code file of a cylinder. The peel test data and color separated regions for “safe”, “transitional”, and “unsafe” regions are shown in Fig. 7a. The working principle for one iteration of the GPSV is shown in Fig. 7b. The resulting color-coded plots of a CAD cylinder indicating peel force are shown in Fig. 7c, with varying degrees of peel force ranges based on print time between layers (increasing with decreasing print speed). The larger the model layer, the longer it will take to print, and therefore the more likely the interfacial layer adhesion will decrease. The goal is certainly to fall within the “safe” category of interfacial adhesion, but reaching that goal may require redesign of the model itself or custom path-planning to ensure that the layers experiencing the most force have

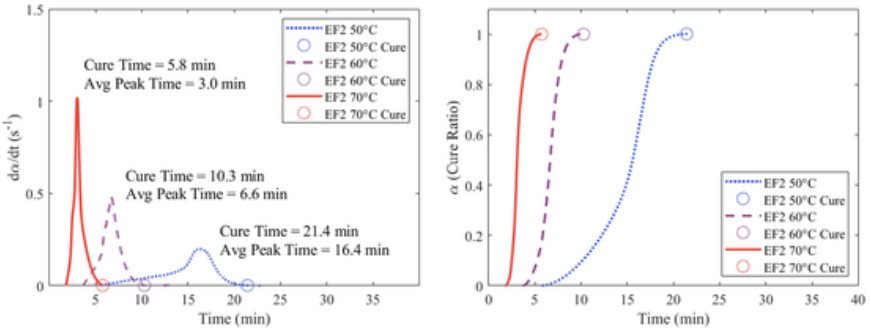

Fig. 4. Curing kinetics results. (left) Averaged isothermal scans of EF with cure time (noted on the graph with circles) and peak cure rate time. (right) Cure percent of EF vs. time, cure time noted on the graph with circles.

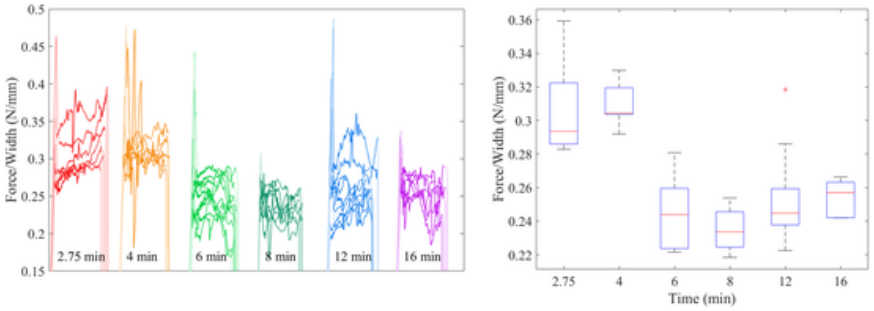

Fig. 5. Peel test results. (left) Sample data per time. (right) Box plot of peel data not including initialization peak and post-break data.

Table 1
Peel test values. Overall peel test data in terms of layer 1 cure time and layer 1 cure percent before deposition of the second layer. Peel forces are separated into "high" and "low" force regions.

Force region	Sample time (min)	Cure % before 2nd Layer	Average max (N/mm)	Average mean (N/mm)
High	2.75	0	0.382 + /-0.064	0.307 + /-0.028
High	4	0.4	0.392 + /-0.063	0.310 + /-0.013
Low	6	24	0.318 + /-0.068	0.245 + /-0.022
Low	8	90	0.270 + /-0.019	0.235 + /-0.013
Low	12	100	0.358 + /-0.089	0.253 + /-0.029
Low	16	100	0.310 + /-0.024	0.253 + /-0.011

higher levels of adhesion. The strategy for coloring each point on the model according to adhesion safety can be logically extended to other shapes. As print speed increases, the cylinder takes less time to print and therefore the geometry's volume falls in the safe region of peel forces. Print time is the simplest variable to change when trying to adjust for specific peel force values, unless the required size of the part can somehow be changed. Each region's safety designation can be altered to reflect specific user design requirements. More complex G-code and advanced path planning methods are required to take full advantage of this peel test data, including horizontal adhesion between lines and multiple-line adhesion from layer-to-layer.

4. Discussion

Without full knowledge of the reasons why mechanical properties vary in a direct ink written part, the printing process development is incomplete. The development process for this printing system is complex because it relies on many interconnected parameters. However, predicting interfacial adhesion forces is one piece of the development puzzle that enables part designers to estimate how printed parts may behave under tension. As mentioned previously, interfacial adhesion characterization must also be integrated into the path planning system, which is its own separate part of printer usability development. For example, it may be possible to design portions of the print to fail earlier than others under the same stress, or to ensure all layers have the same adhesive force for the part to function properly. This is not a trivial problem, especially when using more complex CAD models.

The peel data in this work may seem straightforward to those working in polymer science. With lower silicone cure between layers, there are simply more covalent bonds and potentially other attractive forces, and as the cure percent increases, these available bonds and forces decrease to a plateau. However, these adhesion principles are not yet implemented in direct ink writing systems, as many printers are still in the lab bench phase. This type of work is needed to increase the quality of DIW prints. Because directly measuring adhesion in a printed filament is a difficult proposition, the design of a custom test setup for peeling apart thin printed filaments is left to future work.

This work is limited to studying the adhesion effects from 2.75 min (0% cure) and onward due to the time required to mix and spread the films by hand. This 0% cure value comes from the DSC data, which at 60 °C unfortunately does not reach a positive cure rate until just over three minutes. This is because the samples were not pre-heated – this was done to capture as much quantifiable curing data in the furnace as possible and reduce the amount of curing during prep outside the DSC. At room temperature (25 °C), Ecoflex 00-30 takes four hours to cure [46], so two minutes (0.83% of that time) is unlikely to produce a significant cure effect during sample preparation. Keeping the samples at temperature during mixing, transfer to a syringe, measuring, loading into the pan, and clamping the pan would be unreasonable at 60 °C. So, each sample required a short period of time to heat up inside the DSC furnace before heat flow values passed over the cure baseline value.

Cure state of the mixed silicone should also be discussed in the context of the printer's in-line mixer. There is a high rate of variability in the flow rates potentially possible for this type of printing because each user may use a different nozzle and print speed. However, initial tests in this system at 60 °C suggest a flow rate range of 0.2–0.8 mL/min (approximately 45–11 s in this mixer) to avoid clogging at the lower flow rates and ensure curing at the higher flow rates. More information about the mixer geometry and flow rate decisions are in Figs. A11–A13. The short residence time range means that the mixed silicone is theoretically less cured immediately upon exit than what was testable for peel testing. However, this silicone has been shown to hold structure even immediately upon exit (Video A1) and the interfacial bonding will be theoretically as high or higher than the peel test data currently shown.

It is important to note that the quality of a silicone-printed CAD model is highly reliant on several interdependent parameters, including: print speed, flow rate of the silicone fluid, layer height, layer width, CAD model overhang, model spanning, exterior wall thickness (if hol-

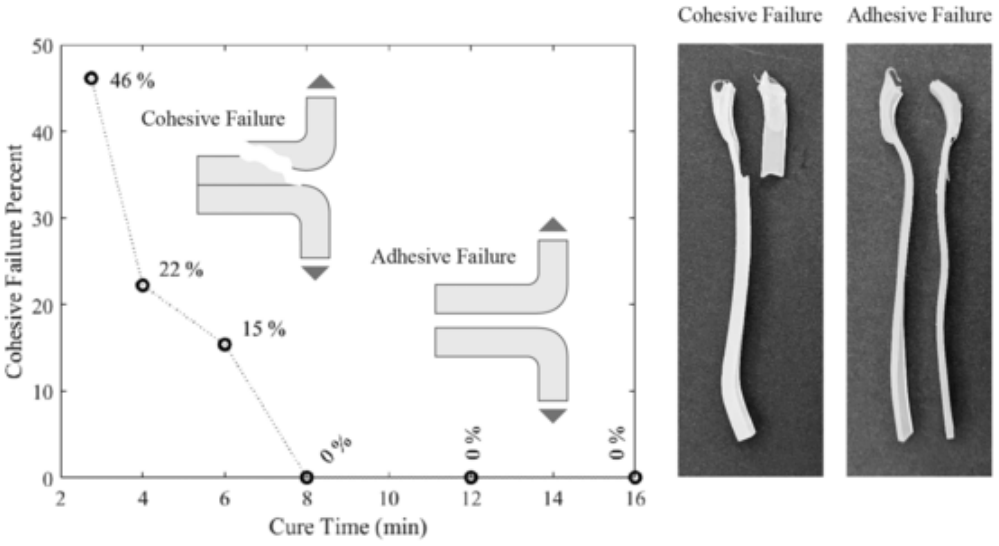

Fig. 6. (left) Cohesive failure (failure in the bulk material) percentages for all samples. (right) Examples of cohesive and adhesive failure in two different tested samples.

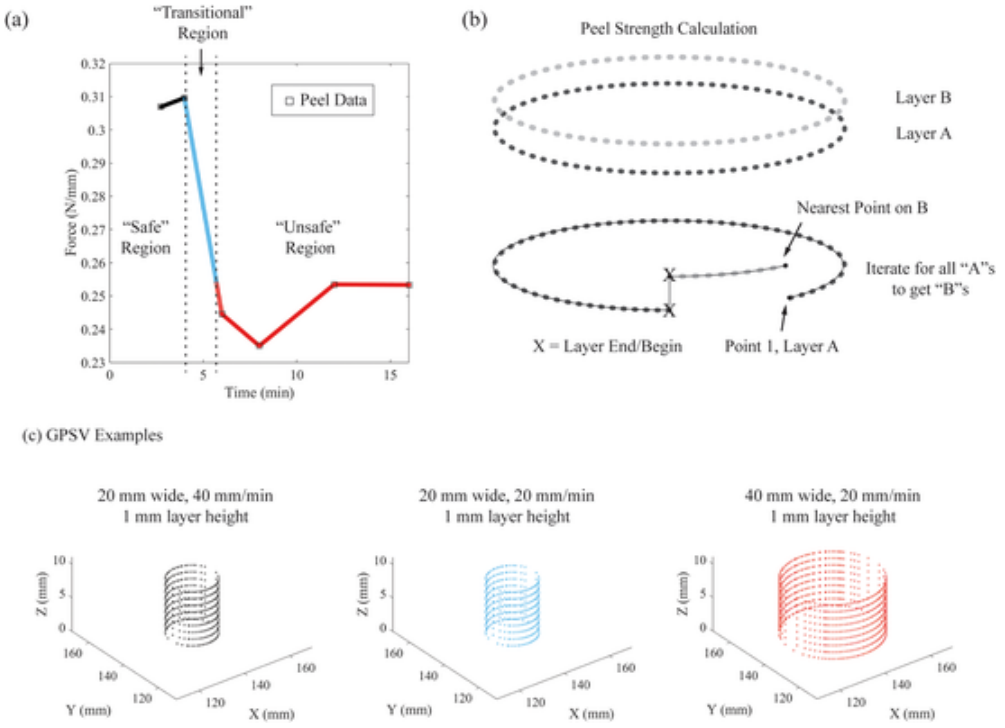

Fig. 7. GPSV results (a) peel test data interpolated to form regions of good (safe) peel forces, transitional peel forces, and lower (unsafe) peel forces. (b) Peel strength value calculations are based on time from point-to-point on Layer A (bottom layer) to Layer B (layer just above A). (c) The GPSV code output is a visualization showing points color-coded to indicate the peel force values for a single-wall cylindrical prints similar to the print shown in Fig. 1b. Print speed can be increased, or model size decreased, to increase expected peel force.

low), and G-code specified path planning. Future work on this printing system will further characterize these relationships.

Peel test results did show some variation, especially in the maximum peel force values that included the initiation peak (Table 1). At this point the reason for jagged variation in the region after initiation is unknown, except that the forces measured are relatively small so small force changes are more obvious, and the deposition was performed in a regular lab environment (not a clean room) which may allow some particulate to settle between the uncured layers. There may also be uneven additive distribution on the small-scale which may change the peel behavior. The standard deviations in the solid line "average" region were between 0.011 and 0.029 N/mm. Because of the low measured force values, a more sensitive instrument to perform peel testing may be needed in the future to clarify these results and also to peel apart small printed filament samples. Peel test results could have also been affected by several factors along with difficulty of film spreading: (1) gravitational forces causing bending in the sample end, (2) unevenness in the placement of the acetate layer boundary causing a slightly non-perpendicular start to the peel initiation area, or (3) uneven widths of samples due to hand-cutting methods Nevertheless, the concept of decreasing interfacial peel force with increasing cure time between layers is clearly indicated in the data, with differences between the higher and lower region means. These force differences will be even more apparent in prints with large interfacial surface areas.

For this DIW system with in-line mixing which cures while printing, final tensile strength from interfacial adhesion between two curing materials will change based on previous layer percent cure before subsequent layer attachment. Here, the adhesive force required to separate two layers of silicone is higher when the layer is deposited before 0.4% cure (4 min). For the silicone direct ink writing system, this four-minute boundary for higher strength parts limits the cross-sectional surface area in a single printed layer to smaller regions and/or to faster printing speeds. This peel force boundary will be investigated in future work with more time increments between 4 and 6 min of cure. The decrease in peel force was expected as the silicone cure percent increased, but it is unclear why the uptick occurs in peel force after 8 min of cure time. This increase could be attributed to bloom or chemical additive migration, where components in a rubber reach their solubility limit inside the bulk material and migrate to the surface over time [47]. Addition cure chemistries like Ecoflex 00-30 do not make any byproducts, but in this work we are using several additives which could cause this effect. Their influence in the increase in peel strength is currently unknown, and is left to future work.

The break points between the peel force values in the "safe", "transitional", and "unsafe" regions can be changed to fit specific use cases. For example, the safe value for one part designer may encompass the entire range of peel forces, and thus the cure state of the layer does not affect final mechanical properties; or the "safe" value may be moved much farther along in the cure time, because the part will experience lower levels of stress. These values are easily viewable in the current GPSV iteration.

Control of the curing process to create predictable interfacial forces throughout the printed part can be a difficult proposition, especially with arbitrary, asymmetric geometries. This is why it is so important to integrate peel data into the printer path planning design early in its development. Fully predictable DIW print mechanics require considering the complexities of interfacial strength, in addition to cure rate, mixing quality, and rheology. These procedural considerations can be implemented with advanced path planning techniques to print new layers on top of acceptable cure percent regions in lower printed layers. Knowing the interfacial peel force can also help print process designers modify

print chamber temperature or make chemical modifications to enable in-line mixing DIW without stopping the cure progression completely.

5. Conclusions

Building on the framework for DIW of curing thermoset silicone [14], this work characterized the interfacial adhesive peel forces in silicone layers of varying cure percent. Interfacial adhesive forces decreased with increasing cure percent between deposited silicone layers. DSC data for potential printing temperatures at 50 °C, 60 °C, and 70 °C quantified cure rate and cure percent growth in a silicone thermoset elastomer (Ecoflex 00-30 mixture) to compare with T-Peel test data. With a 60 °C printer chamber temperature, layers with less than 0.4% cure (high force region) had a higher peel force than layers with 24% cure or more (low force region). A G-code Peel Strength Visualizer was written in MATLAB to show the effect of time on peel forces between part layers. Iterations on path planning using this code will be useful for silicone DIW workflow. Overall, this work emphasizes the importance of incorporating interfacial adhesion data into in-line mixed DIW printer systems to enable predictable tensile performance in DIW parts.

CRediT authorship contribution statement

Stephanie Walker: Conceptualization, Methodology, Visualization, Writing – original draft, Writing – review & editing, Investigation, Software. **Emma Lingle:** Investigation. **Natasha Troxler:** Investigation. **T.J. Wallin:** Writing – review & editing, Supervision. **Katherine Healy:** Writing – review & editing, Supervision. **Yiğit Mengüç:** Writing – review & editing, Supervision. **Joseph Davidson:** Writing – review & editing, Supervision, Project administration.

Declaration of Competing Interest

The authors declare that they have no known competing financial interests or personal relationships that could have appeared to influence the work reported in this paper.

Acknowledgments

This work was supported by a sponsored research agreement with Facebook Technologies, LLC (proposal no. 19-1897). Representatives for Facebook Reality Labs have made suggestions for study conceptual design, provided writing and editing support, and have approved this manuscript for publication.

Appendix A. Supporting information

Supplementary data associated with this article can be found in the online version at doi:10.1016/j.addma.2021.102320.

References

[1] M.A. Skylar-Scott, J. Mueller, C.W. Visser, J.A. Lewis, Voxelated soft matter via multimaterial multinozzle 3D printing, Nature 575 (2019) 330–335, https://doi.org/10.1038/s41586-019-1736-8.
[2] H. Yuk, X. Zhao, A new 3D printing strategy by harnessing deformation, instability, and fracture of viscoelastic inks, Adv. Mater. (2017) 1704028, https://doi.org/10.1002/adma.201704028.
[3] T.J. Ober, D. Foresti, J.A. Lewis, Active mixing of complex fluids at the microscale, Proc. Natl. Acad. Sci. 112 (2015) 12293–12298, https://doi.org/10.1073/pnas.1509224112.
[4] T.J. Hinton, A. Hudson, K. Pusch, A. Lee, A.W. Feinberg, 3D printing pdms elastomer in a hydrophilic support bath via freeform reversible embedding, ACS Biomater. Sci. Eng. 2 (2016) 1781–1786, https://doi.org/10.1021/acsbiomaterials.6b00170.
[5] T. Bhattacharjee, S.M. Zehnder, K.G. Rowe, S. Jain, R.M. Nixon, W.G. Sawyer, T.E. Angelini, Writing in the granular gel medium, Sci. Adv. 1 (2015) 1500655, https://doi.org/10.1126/sciadv.1500655.
[6] C.S. O'Bryan, T. Bhattacharjee, S. Hart, C.P. Kabb, K.D. Schulze, I. Chilakala, B.S. Sumerlin, W.G. Sawyer, T.E. Angelini, Self-assembled micro-organogels for 3D printing silicone structures, Sci. Adv. 3 (2017) 1602800, https://doi.org/10.1126/sciadv.1602800.
[7] A. Frutiger, J.T. Muth, D.M. Vogt, Y. Mengüç, A. Campo, A.D. Valentine, C.J. Walsh, J.A. Lewis, Capacitive soft strain sensors via multicore–shell fiber printing, Adv. Mater. 27 (2015) 2440–2446, https://doi.org/10.1002/adma.201500072.
[8] J.O. Hardin, T.J. Ober, A.D. Valentine, J.A. Lewis, Microfluidic printheads for multimaterial 3D printing of viscoelastic inks, Adv. Mater. 27 (2015) 3279–3284, https://doi.org/10.1002/adma.201500222.
[9] S. Roh, D.P. Parekh, B. Bharti, S.D. Stoyanov, O.D. Velev, 3D printing by multiphase silicone/water capillary inks, Adv. Mater. 29 (2017) 1701554, https://doi.org/10.1002/adma.201701554.
[10] F.B. Coulter, A. Ianakiev, 4D printing inflatable silicone structures, 3D print, Addit. Manuf. 2 (2015) 140–144, https://doi.org/10.1089/3dp.2015.0017.
[11] F.B. Coulter, M. Schaffner, J.A. Faber, A. Rafsanjani, R. Smith, H. Appa, P. Zilla, D. Bezuidenhout, A.R. Studart, Bioinspired heart valve prosthesis made by silicone additive manufacturing, Matter 1 (2019) 266–279, https://doi.org/10.1016/j.matt.2019.05.013.
[12] M.M. Durban, J.M. Lenhardt, A.S. Wu, W. Small, T.M. Bryson, L. Perez-Perez, D.T. Nguyen, S. Gammon, J.E. Smay, E.B. Duoss, J.P. Lewicki, T.S. Wilson, Custom 3D printable silicones with tunable stiffness, Macromol. Rapid Commun. 39 (2018) 1700563, https://doi.org/10.1002/marc.201700563.
[13] J.I. Lipton, S. Angle, H. Lipson, 3D printable wax-silicone actuators, in: proceedings of the 2014 Annual International Solid Freeform Fabrication Symposium, Laboratory for Freeform Fabrication and University of Texas Austin, TX, 2014: pp. 4–6.
[14] S. Walker, U. Daalkhaijav, D. Thrush, C. Branyan, O.D. Yirmibesoglu, G. Olson, Y. Menguc, Zero-support 3D printing of thermoset silicone via simultaneous control of both reaction kinetics and transient rheology, 3D print, Addit. Manuf. 6 (2019) 139–147, https://doi.org/10.1089/3dp.2018.0117.
[15] S. Walker, O.D. Yirmibeşoğlu, U. Daalkhaijav, Y. Mengüç, Additive manufacturing of soft robots, in: S.M. Walsh, M.S. Strano (Eds.), Robotic Systems and Autonomous Platforms, Woodhead Publishing, 2019, pp. 335–359, https://doi.org/10.1016/B978-0-08-102260-3.00014-7.
[16] M.K. Chaudhury, A.V. Pocius, D.A. Dillard, Adhesion Science and Engineering: Surfaces, Chemistry and Applications, Elsevier Science & Technology, Amsterdam,, NETHERLANDS, THE, 2002 ⟨http://ebookcentral.proquest.com/lib/osu/detail.action?docID=317137⟩, accessed November 12, 2020.
[17] Slic3r Manual – Flow Math, (n.d.). ⟨https://manual.slic3r.org/advanced/flow-math⟩ (accessed August 24, 2020).
[18] P. Mazurek, S. Vudayagiri, A.L. Skov, How to tailor flexible silicone elastomers with mechanical integrity: a tutorial review, Chem. Soc. Rev. 48 (2019) 1448–1464, https://doi.org/10.1039/C8CS00963E.
[19] K. Dušek, Diffusion control in the kinetics of cross-linking, Polym. Gels Netw. 4 (1996) 383–404, https://doi.org/10.1016/S0966-7822(97)89914-5.
[20] T.R.E. Simpson, B. Parbhoo, J.L. Keddie, The dependence of the rate of crosslinking in poly(dimethyl siloxane) on the thickness of coatings, Polymer 44 (2003) 4829–4838, https://doi.org/10.1016/S0032-3861(03)00496-8.
[21] I.-K. Hong, S. Lee, Cure kinetics and modeling the reaction of silicone rubber, J. Ind. Eng. Chem. 19 (2013) 42–47, https://doi.org/10.1016/j.jiec.2012.05.006.
[22] J. Studer, C. Dransfeld, K. Masania, An analytical model for B-stage joining and co-curing of carbon fibre epoxy composites, Compos. Part Appl. Sci. Manuf. 87 (2016) 282–289, https://doi.org/10.1016/j.compositesa.2016.05.009.
[23] TA Instruments, A Review of DSC Kinetics Methods (TA073), (n.d.). ⟨http://www.tainstruments.com/pdf/literature/TA073.pdf⟩ (accessed September 14, 2017).
[24] S. Sourour, M.R. Kamal, Differential scanning calorimetry of epoxy cure: isothermal cure kinetics, Thermochim. Acta 14 (1976) 41–59, https://doi.org/10.1016/0040-6031(76)80056-1.
[25] R.J. Young, P.A. Lovell, Introduction to Polymers, CRC Press,, 2011.
[26] K.E. Polmanteer, C.W. Lentz, Reinforcement studies—effect of silica structure on properties and crosslink density, Rubber Chem. Technol. 48 (1975) 795–809, https://doi.org/10.5254/1.3539687.
[27] H. Cochrane, C.S. Lin, The influence of fumed silica properties on the processing, curing, and reinforcement properties of silicone rubber, Rubber Chem. Technol. 66 (1993) 48–60, https://doi.org/10.5254/1.3538299.
[28] L.-H. Cai, T.E. Kodger, R.E. Guerra, A.F. Pegoraro, M. Rubinstein, D.A. Weitz, Soft poly(dimethylsiloxane) elastomers from architecture-driven entanglement free design, Adv. Mater. 27 (2015) 5132–5140, https://doi.org/10.1002/adma.201502771.
[29] D14 Committee, Test Method for Peel Resistance of Adhesives (T-Peel Test), ASTM International, n.d. ⟨https://doi.org/10.1520/D1876-08R15E01⟩.
[30] N. Padhye, D.M. Parks, A.H. Slocum, B.L. Trout, Enhancing the performance of the T-peel test for thin and flexible adhered laminates, Rev. Sci. Instrum. 87 (2016) 085111, https://doi.org/10.1063/1.4960172.
[31] A.J. Kinloch, J.G. Williams, The mechanics of peel tests, Adhesion Science and Engineering, Elsevier, 2002, pp. 273–301, https://doi.org/10.1016/B978-0-444-51140-9.50035-4.
[32] M. Rezaee, L.-C. Tsai, M.I. Haider, A. Yazdi, E. Sanatizadeh, N.P. Salowitz, Quantitative peel test for thin films/layers based on a coupled parametric and statistical study, Sci. Rep. 9 (2019) 19805, https://doi.org/10.1038/s41598-019-55355-9.
[33] A. Chiche, W. Zhang, C.M. Stafford, A. Karim, A new design for high-throughput peel tests: statistical analysis and example, Meas. Sci. Technol. 16 (2005) 183–190, https://doi.org/10.1088/0957-0233/16/1/024.
[34] S. Ebnesajjad, C. Ebnesajjad, Surface Treatment of Materials for Adhesive Bonding,

Elsevier Science & Technology Books,, Norwich, United States, 2013 ⟨http://ebookcentral.proquest.com/lib/osu/detail.action?docID=1495678⟩, accessed July 12, 2020.
[35] J. Morrow, S. Hemleben, Y. Menguc, Directly fabricating soft robotic actuators with an open-source 3-D printer, IEEE Robot. Autom. Lett. 2 (2017) 277–281, https://doi.org/10.1109/LRA.2016.2598601.
[36] O.D. Yirmibesoglu, J. Morrow, S. Walker, W. Gosrich, R.A. Canizares, H. Kim, U. Daalkhaijav, C. Fleming, C. Branyan, Y. Menguc, Direct 3D printing of silicone elastomer soft robots and their performance comparison with molded counterparts, in: proceedings of the 2018 IEEE International Conference on Soft Robotics, RoboSoft. (2018).
[37] C. Schmidleithner, D.M. Kalaskar, Stereolithography, in: D. Cvetković (Ed.), 3D Print, InTech, 2018, https://doi.org/10.5772/intechopen.78147.
[38] D. McCoul, S. Rosset, S. Schlatter, H. Shea, Inkjet 3D printing of UV and thermal cure silicone elastomers for dielectric elastomer actuators, Smart Mater. Struct. 26 (2017) 125022, https://doi.org/10.1088/1361-665X/aa9695.
[39] ACEO® - Unique Drop on Demand Technology with 70 Years of Silicone Knowhow, (n.d.). ⟨https://www.aceo3d.com/technology/⟩ (accessed March 31, 2020).
[40] A.D. Benjamin, R. Abbasi, M. Owens, R.J. Olsen, D.J. Walsh, T.B. LeFevre, J.N. Wilking, Light-based 3D printing of hydrogels with high-resolution channels, Biomed. Phys. Eng. Express 5 (2019) 025035, https://doi.org/10.1088/2057-1976/aad667.
[41] D.R. Smalley, T.J. Vorgitch, C.R. Manners, C.W. Hull, S.L. VanDorin, Simultaneous multiple layer curing in stereolithography, US5597520A, 1997. ⟨https://patents.google.com/patent/US5597520A/en⟩ (accessed March 27, 2020).
[42] H. Kodama, Automatic method for fabricating a three-dimensional plastic model with photo-hardening polymer, Rev. Sci. Instrum. 52 (1981) 1770–1773, https://doi.org/10.1063/1.1136492.
[43] S.A. Morin, S.W. Kwok, J. Lessing, J. Ting, R.F. Shepherd, A.A. Stokes, G.M. Whitesides, Elastomeric tiles for the fabrication of inflatable structures, Adv. Funct. Mater. 24 (2014) 5541–5549.
[44] A.D. Marchese, C.D. Onal, D. Rus, Autonomous soft robotic fish capable of escape maneuvers using fluidic elastomer actuators, Soft Robot. 1 (2014) 75–87, https://doi.org/10.1089/soro.2013.0009.
[45] R.F. Shepherd, F. Ilievski, W. Choi, S.A. Morin, A.A. Stokes, A.D. Mazzeo, X. Chen, M. Wang, G.M. Whitesides, Multigait soft robot, Proc. Natl. Acad. Sci. 108 (2011) 20400–20403, https://doi.org/10.1073/pnas.1116564108.
[46] EcoflexTM 00–30 Product Information, Smooth-Inc. (n.d.). ⟨https://www.smooth-on.com/products/ecoflex-00–30/⟩ (accessed July 12, 2020).
[47] F. Ignatz-Hoover, B.H. To, R.N. Datta, A.J. de Hoog, Chemicaladditives migration in rubber, Rubber Chem. Technol. 76 (2003) 747–768.